Scaffold-free Bioprinting of Mesenchymal Stem Cells Using the Regenova Printer: Spheroid Characterization and Osteogenic Differentiation

*Izath Nizeet Aguilar[1], *David J. Olivos, III[2], Alexander Brinker[1], Marta B. Alvarez[1], Lester J. Smith[3],Tien-Min Gabriel Chu[1,4,5], Melissa A. Kacena[1], Diane R. Wagner[6**]

1 Department of Orthopaedic Surgery, Indiana University School of Medicine, Indianapolis, IN 46202, USA
2 Department of Biochemistry and Molecular Biology, Indiana University of School of Medicine, Indianapolis, Indiana, USA
3 Department of Radiology and Imaging Sciences, Indiana University of School of Medicine, Indianapolis, Indiana, USA
4 Weldon School of Biomedical Engineering, Purdue University, West Lafayette, IN 47908, USA
5 Department of Biomedical and Applied Sciences, Indiana University School of Dentistry, Indianapolis, IN 46202, USA
6 Department of Mechanical and Energy Engineering, Indiana University Purdue University Indianapolis, Indianapolis, Indiana, USA

*Izath Nizeet Aguilar and David J. Olivos III contributed equally to this work

****Corresponding Author and Lead Contact:**

Diane R. Wagner, Ph.D.
Associate Professor
Indiana University-Purdue University Indianapolis, IN, USA
Department of Mechanical and Energy Engineering
SL 164D
Indianapolis IN 46202
(317) 274-8958– phone
wagnerdi@iupui.edu

Keywords
Osteogenesis
Mesenchymal Stem Cells
Spheroid Formation
Bioprinting
Scaffold-Free
Tissue Engineering
Regenova

This is the author's manuscript of the article published in final edited form as:

Aguilar, I. N., Olivos, D. J., Brinker, A., Alvarez, M. B., Smith, L. J., Chu, T.-M. G., … Wagner, D. R. (2019). Scaffold-free bioprinting of mesenchymal stem cells using the Regenova printer: Spheroid characterization and osteogenic differentiation. Bioprinting, 15, e00050. https://doi.org/10.1016/j.bprint.2019.e00050

Abstract

Limitations in scaffold material properties, such as sub-optimal degradation time, highlight the need for alternative approaches to engineer *de novo* tissues. One emerging solution for fabricating tissue constructs is scaffold-free tissue engineering. To facilitate this approach, three-dimensional (3D) bioprinting technology (Regenova Bio 3D Printer) has been developed to construct complex geometric shapes from discrete cellular spheroids without exogenous scaffolds. Optimizing spheroid fabrication and characterizing cellular behavior in the spheroid environment are important first steps prior to printing larger constructs. Here, we characterized spheroids of immortalized mouse bone marrow stromal cells (BMSCs) that were differentiated to the osteogenic lineage.

Immortalized BMSCs were seeded in low attachment 96-well plates in various numbers to generate self-aggregated spheroids either under the force of gravity or centrifugation. Cells were cultured in control or osteogenic media for up to 28 days. Spheroid diameter, roundness and smoothness were measured. Cell viability, DNA content and alkaline phosphatase activity were assessed at multiple time points. Additionally, expression of osteogenic markers was determined using real time qPCR.

Spheroids formed under gravity with 20K, 30K and 40K cells had average diameters of 498.5 ± 8.3 μm, 580.0 ± 32.9 μm and 639.2 ± 54.0 μm, respectively, while those formed under 300G centrifugation with the same numbers of cells had average diameters of 362.3 ± 3.5 μm, 433.1 ± 6.4 μm and 491.2 ± 8.0 μm. Spheroids formed via centrifugation were superior to those formed by gravity, as evidenced by better roundness and smoothness and double the retention of DNA (cellular) content. Cells in spheroids exhibited a robust osteogenic response to the differentiation medium, including higher mRNA expression of alkaline phosphatase, collagen type I, and osteocalcin than those cultured in control medium, as well as greater alkaline phosphatase activity. The optimal spheroid fabrication technique from this study was to

aggregate 40K cells under 150 – 300G centrifugation. In future investigations, these spheroids will be 3D printed into larger tissue constructs.

1. Introduction

The majority of tissue engineering methods utilize exogenous biocompatible scaffolds to support cell attachment onto precisely designed templates, but several challenges persist in tissue engineering with these methods. The selection of an appropriate scaffold is important as many issues such as cell-cell communication, cell-ECM/scaffold communication, immunogenicity, toxicity, inflammation, and mechanical incompatibility are directly determined by scaffold properties[1–3]. One of the limitations of tissue engineering approaches using exogenous scaffolds is degradation time. A fast-kinetic degradation scaffold may produce byproducts (acidic, basic, or otherwise deleterious) at a concentration too high for the surrounding tissue to resorb, and can affect the viability of the cells. Alternately, scaffolds that do not degrade quickly enough may hinder matrix production[2,4,5]. Scaffold-free engineering methods provide alternative assembly systems for generating new tissues[2,6–8]. Using the scaffold-free method, cells secrete the extracellular matrix required to provide structure. Therefore, the cells are within a biologically optimized extra-cellular matrix (ECM) environment to which they are suited. The utilization of cell-secreted ECM also eliminates the need to rely on the degradation of synthetic scaffold materials.

The Regenova Bio 3D Printer from Cyfuse facilitates the high-resolution fabrication of scaffold-free tissue engineered constructs in custom shapes by three-dimensional (3D) printing scaffold-free cellular spheroids[9–13]. The appeal of 3D printing resonates with its relative ease of generating a particular 3D geometry and the accuracy of situating cellular spheroids in a pre-designed spatial location. The Regenova system has been used to construct various tissues associated with the vasculature, tracheal tissue, and to regenerate cartilage defects with high-

density mesenchymal stem cells[9,10,12,13]. The Regenova system sets itself apart from other 3D bioprinters by skewering individual cellular spheroids into a predetermined design onto an array of stainless steel needles (170 µm in diameter in either a 9x9 or a 26x26 pattern) called a Kenzan. This "Kenzan method" does not use a scaffold for final structural support, but relies instead on natural cell-to-cell contact behavior (e.g. cadherin-mediated adhesion, integrins, connexins, and adherence junctions), to facilitate spheroid fusion[14,15], resulting in a larger tissue construct. The secretion of ECM adds structural integrity to the construct as it matures[16–21]. The cellular spheroids form the building blocks of the tissue and must provide an environment that supports extracellular matrix deposition and the maintenance of metabolic functions[22].

In order to create 3D tissues with the Regenova Bio 3D Printer, the spheroid formation has to be optimized to a target diameter of 500 µm with an acceptable range of ~450-550 µm and appropriate symmetry and strength to successfully survive automated retrieval and organized placement during printing. While the optimal spheroid size for Kenzan bioprinting with this device is 500 µm (figure 1(a)), spheroids as large as 1 mm can be picked up, and spheroids as large as 800 µm have been printed using the Regenova. However, large spheroids interfere with one another during the printing process such that, when printed adjacent to one another, each spheroid will push the preceding spheroid down the needle, changing the construct shape and dimensions, and risking spheroid rupture (figures 1(b) and (c)). Additionally, oversized spheroids may distort the spacing between the needles in the array as printing progresses from the bottom to the top of the Kenzan. Therefore, the use of large spheroids may only be suitable for general printability testing and to determine spheroid behavior post-printing. Undersized spheroids (400 µm or less) may be difficult to pick up and high numbers of spheroids may fail to print due to splitting as they are placed over the Kenzan needles (figure 1(d)). Furthermore, center-to-center needle spacing on the Kenzan needles is 400 µm. Therefore, undersized spheroids cannot span the needle gap and contact one another, such that spheroid-spheroid fusion, integral to post-printing construct maturation, may not occur.

In this study we focused on characterizing spheroids for use in the Regenova Bio 3D printer and the Kenzan method of biofabrication to develop a bone tissue construct for craniofacial reconstruction. It is estimated that 17 million surgeries in the craniofacial region are performed in the United States[23,24]. Difficulties repairing cranial bone defects caused by severe trauma, infection and congenital deformity remain a major challenge to cranial surgeons[25]. These procedures heavily rely on archaic techniques currently available to surgeons, which include utilizing foreign materials such as metal plates, bone cement, and stainless-steel grids for reinforcement[26–28]. Anatomically correct reconstruction of highly complex craniofacial shape is challenging; the ability to engineer anatomically correct tissues with viable and functional cells would have tremendous potential for bone reconstructions[26–28]. Here, we use immortalized mouse bone marrow stromal cells (BMSCs) which have been previously characterized in terms of their osteogenic properties under two-dimensional (2D) culture conditions[29]. We compared methods of spheroid formation by centrifugation-assisted aggregation and gravity-assisted aggregation, and analyzed the resulting spheroids for viability, osteogenic activity in 3D structures and suitability for printing. This study provides a detailed optimization of BMSC spheroids for use in the bioprinting of larger constructs using the Regenova Bio 3D Printer robotics system by Cyfuse.

2. Methods

2.1 Bone marrow derived stromal cell (BMSC) culture

Immortalized BMSCs were generated from C57BL/6 mice as previously described by Alvarez et al[29]. Briefly, immortalized wild-type clones were selected based on their positive staining for alkaline phosphatase and capacity for mineralization[29]. Frozen BMSCs were thawed, expanded, and cultured in control medium (Alpha-Minimum Essential Medium (α-MEM, Gibco ®, NY, USA), 10% fetal bovine serum (Atlas Biologicals, CO, USA), 1% penicillin-streptomycin-glutamate (Gibco ®, NY, USA), and 0.001% amphotericin B (Sigma-Aldrich,

MO,USA). For cell passaging, cells were cultured up to 90% confluence and then were detached with trypsin-EDTA (0.25%, Gibco ®) and were seeded into new dishes or used for generation of spheroids as described below.

2.2 Spheroid formation

Gravity-induced spheroids (Passage 31) were generated by seeding BMSC in Ultra Low Attachment (ULA) U-bottom 96 well plates (SBIO^{TM}, Japan). Different cell concentrations were seeded (5K, 10K, 15K, 20K, 30K and 40K) to generate spheroids with a target diameter between 450 to 550 µm at day 3. BMSC spheroids were cultured in control medium or in the same medium supplemented with 50 mg/ml of L-ascorbic acid 2-phosphate (Sigma-Aldrich) and 200 mM β-glycerophosphate disodium salt hydrate (Sigma-Aldrich), referred to as osteogenic medium. Media were changed three times per week.

Centrifuge-induced spheroids (Passage 36) were generated by adding 20K, 30K, 40K or 50K BMSC cells/well in ULA U-bottom 96 well plates, under the same media conditions, but plates were centrifuged for 5 min at 150G or 300G immediately after cell seeding.

Both gravity- and centrifuge-induced spheroids were cultured for up to 28 days. Spheroid diameter, roundness and smoothness were measured with the Regenova Bio 3D Printer scanner (Regenova Bio 3D Printer, Cyfuse, K.K., Japan) at various time points. Roundness was calculated by the Regenova 3D Printer from the radius of the smallest circumscribed circle of the spheroid (*R*) and the radius (*r*) of an inscribed circle, concentric with the first circle, and contacting the spheroid perimeter. Roundness was then calculated using the following equation:

$$Roundness[\%] = \left[100 - \left(\frac{(R-r)}{R}\right)\right] * 100 \quad (1)$$

Smoothness was determined by measuring the area of the regions deviating from the average of the minimum and maximum contour of the spheroid (*DA*) and then dividing by the spheroid area (*SA*):

$$Smoothness[\%] = \frac{DA}{SA} * 100$$

(2)

The exponential decay model parameters were fit to the spheroid diameter data using SigmaPlot (Systat Software Inc., CA, USA):

$$D(t) = D_{eq}\left(1 + e^{\left(-\frac{(t)}{\tau}\right)}\right), \quad (3)$$

where D_{eq} is the diameter at equilibrium, t is time, and τ is the exponential time constant.

2.3 Cell Viability and Spheroid Morphology

Gravity-induced spheroids composed of 20K cells were harvested at time points up to 11 days and were dissociated with 2% collagenase type 2 (Worthington Biochemical Corporation, NJ, USA) in α-MEM for 60 minutes. The percentage of viable cells in each spheroid was assessed by counting cells excluding Trypan Blue Stain (0.4%; Gibco ®) with a hemocytometer (n=4), dividing by the total number of counted cells and then multipling by 100%.

Spheroids were fixed with 10% neutral buffered formalin for 24 hours before being encapsulated in 2% agarose for 10 minutes to facilitate handling. Spheroids were then stored in 70% ethanol until they were embedded in paraffin, sectioned, and stained with Hematoxylin and Eosin (H&E) and imaged under light microscopy with 10X and 40X objectives.

2.4 Reverse Transcription-Quantitative Polymerase Chain Reaction (RT-qPCR)

Total RNA was isolated by pooling 8 gravity-induced spheroids per replicate (n=3) that had been cultured in osteogenic or control medium using the RNeasy® Plus Mini Kit (Qiagen, MD, USA), according to the manufacturer's protocol, at days 3, 7, 11, 14, 21 and 28. Aliquots of cell suspension with the appropriate cell density were collected on day 0. cDNA was generated with Transcriptor First Strand cDNA Synthesis Kit (Roche Life Science, IN, USA). qPCR was performed using SYBR Master Mix (Life Technology, CA, USA) to assess the expression of osteogenic differentiation markers alkaline phosphatase (ALP), collagen type I (COL 1A1), and

osteocalcin (OCN), which were normalized against glyceraldehyde-3-phosphate dehydrogenase (GAPDH) using the primer sequences in Table 1. The reactions were carried out on the ABI qPCR system (Applied Biosystems, CA, USA). A calibration curve was performed and all oligonucleotides were tested to ensure specificity and sensitivity. For all samples, ΔΔCT method with day 0 as the reference was used for the analysis of the data as previously described[30].

Gene	Forward	Reverse
ALP	5'-GCTGATCATTCCCACGTTTT-3'	5'-CTGGGCCTGGTAGTTGTTGT-3'
COL 1A1	5'-ACGTCCTGGTGAAGTTGGTC-3'	5'-CAGGGAAGCCTCTTTCTCCT-3'
OCN	5'-AAGCAGGAGGGCAATAAGGT-3'	5'-TTTGTAGGCGGTCTTCAAGC-3'
GAPDH	5'-CGTGGGGCTGCCCAGAACAT-3'	5'-TCTCCAGGCGGCACGTCAGA-3'

Table 1: Primer Sequences for RT-qPCR

2.5 DNA Quantification and Alkaline Phosphatase (ALP) Activity

To assess total DNA content, aliquots of cell suspension with the appropriate cell density were collected on day 0 and spheroids of 20K cells each were collected on days 1, 3, 7, 14, 21 and 28. Four spheroids were collected per replicate (n=3) and digested in 0.1% Triton-X (Sigma-Aldrich) with protease inhibitors. The DNA content of samples was assessed via Quant-iT PicoGreen dsDNA Reagent Kit (Invitrogen, CA, USA) following the manufacturer's instructions. DNA content was normalized to the day 0 spheroids. Model parameters of exponential decay were fit to the DNA data using Sigmaplot:

$$DNA(t) = DNA_{eq}\left(1 + e^{\left(-\frac{(t)}{\tau}\right)}\right), \quad (4)$$

where DNA_{eq} is the normalized DNA at equilibrium, t is time, and τ is the exponential time constant.

The same BMSC spheroid digests were assessed for ALP activity using the Alkaline Phosphatase Assay kit (Sigma-Aldrich®) according to the manufactures' protocols. Enzymatic ALP activity was calculated per minute and normalized to DNA content.

2.6 Statistics and Analysis

Unless otherwise indicated, all data are expressed as the mean ± SD. All data were analyzed by a 2-way ANOVA using Tukey's post hoc analysis and $p < 0.05$ as a threshold of statistical significance

3. Results

3.1 Spheroid Diameter and Cell Viability

Different cell concentrations were seeded to generate gravity-induced spheroids with a target diameter of 500 µm on day 3. Spheroids did not form at 5K, 10K and 15K. Spheroids had diameters of 498.5 ± 8.3 µm for 20K cells per well, 580.0 ± 32.9 µm for 30K cells, and 639.2 ± 54.0 µm for 40K cells (figure 2(a)). Gravity-induced spheroids seeded at 20K cells per well were adequate for printing based on spheroid diameter and were used in additional studies.

The Regenova's scanner feature was used to image spheroids cultured in both control and osteogenic media, hereon referred to as control and osteogenic spheroids. On day 1, diameters were 830 ± 107 µm for controls spheroids (n=79) and 785 ± 94 µm for osteogenic spheroids (n=80). The coefficients of exponential decay in equation (3) were fit to the spheroid diameter measurements, with R^2 values of 0.98 and 0.99 for control and osteogenic spheroids, respectively. Spheroid diameters decreased over time before reaching steady state values with τ equal to 2.2 days for both control and osteogenic spheroids. The diameter at equilibrium (D_{eq}) best-fit values of the model for control spheroids was 441 µm and for osteogenic spheroids was

443 μm (figure 2(b) and (c)).The percentage of cells excluding trypan blue was higher than 85% in both groups at all time points examined (figure 2(b) and 2(c)).

3.2 Histology (H&E)

The size of the gravity-induced spheroids decreased over time when cultured in either control or osteogenic medium (upper panel of figure 3; 10X objective). The spheroids produced by gravity on day 1, 2, and 3 were somewhat irregularly shaped. Spheroids cultured in both control and osteogenic medium were highly cellular (lower panel of figure 3; 40X objective).

3.3 mRNA Expression

Spheroids cultured in osteogenic medium expressed higher levels of osteogenic specific genes compared to spheroids cultured in control medium (figure 4). Specifically, ALP mRNA expression was 30-fold and 14-fold higher on day 11 and 14, respectively (figure 4(a)). Likewise, COL 1A1 mRNA expression was significantly higher on days 14 (8-fold increase), 21 (6-fold increase), and 28 (10-fold increase) when spheroids were cultured in osteogenic medium compared to control medium (figure 4(b)). Furthermore, osteogenic spheroids displayed a 16-fold increase of OCN gene expression when compared to control spheroids on day 21, and a 14-fold increase on day 28 (figure 4(c)).

3.4 DNA Content

DNA content analyses were performed on spheroids generated by both gravity and centrifugation. The DNA kinetic profile for gravity- and centrifuge-induced spheroids were similar to the diameter profile (figure 5). The parameters of equation (4) were fit to the DNA kinetic profile with an R^2 higher than 0.90 for both gravity- and centrifuge-induced spheroids. On days 0 and 1, control and osteogenic spheroids showed higher levels of DNA than observed at subsequent time points for both gravity- and centrifuge-induced spheroids. For all groups, the DNA content decreased after day 0 with τ of 2.2 days for both control and osteogenic for gravity-induced spheroids. The exponential decay was shorter for centrifuge-induced spheroids, with τ of 0.2 days for control spheroids and 0.5 days for osteogenic spheroids. Accordingly, the

DNA content approximated steady state by day 3 in gravity-induced spheroids and by day 1 in centrifuge-induced spheroids. Importantly, a greater percentage of DNA content was retained from day 3 to day 28 for centrifuge-induced spheroids compared to that observed for gravity-induced spheroids. Indeed, the equilibrium DNA profile by gravity-induced spheroids decreased approximately 80% from day 0, whereas the equilibrium DNA profile by centrifuge-induced spheroids decreased approximately by 40%. Therefore, spheroids formed via centrifugation were deemed superior to those formed by gravity alone as determined by 2-fold more DNA content retention.

3.5 Spheroid Diameter on Day 3

As a primary goal was to characterize spheroids for use in 3D bioprinting, we next assessed the parameters of importance for this application: diameters ranging between 450 and 550 μm with 500 μm being the target diameter, as well as optimal roundness and smoothness. We determined these properties on day 3 as it was the time point when DNA levels had reached steady state in all cases. Figure 6 (a) shows representative silhouettes of the spheroids that were formed by gravity and centrifugation at different speeds. The spheroids produced via gravity and cell aggregation (20K cells) had a diameter of 498.5 ± 8.3 μm while those formed under centrifugation with the same number of cells had a diameter of 352.3 ± 7.1 μm at 150G and 362.3 ± 3.5 μm at 300G on day 3 (figure 6(b)). Under centrifugation, spheroids formed from 40K cells were the closest to the target diameter of 500 μm, with diameters of 486.1± 7.5 μm and 491.2± 8.0 μm for 150G and 300G, respectively. Spheroids formed by gravity resulted in 17% and 19% less roundness than spheroids formed by the centrifugation method at 150G and 300G, respectively (figure 6(c)). Gravity-induced spheroids were observed with a range of smoothness from 0.0% to 7.1% (0% as the best, 100% as the worst). In comparison, centrifuge-induced spheroids exhibited a range of smoothness from 0.0% to 0.2% (figure 6(d)). The different centrifugation speeds did not have any impact on spheroid diameter, roundness, or smoothness (figure 6(b)-(d)).

3.6 Alkaline Phosphatase Activity

Next, we investigated ALP activity levels in spheroids formed by either gravity or by centrifugation at 300G (20,000 cells/spheroid) and cultured in either control or osteogenic media. Similar to mRNA expression in gravity-induced spheroids, ALP activity significantly increased when spheroids were cultured in osteogenic medium as compared to control medium in both gravity- and centrifuge-induced spheroids (figure 7). Gravity-induced spheroids showed a significant 2.7-fold increase in alkaline phosphatase activity on day 7, a 1.8-fold increase on day 11, a 6.7-fold increase on day 21, and an 8.8-fold increase on day 28 when cultured in osteogenic medium compared to control medium (figure 7(a)). For centrifuge-induced spheroids, there was a significant 1.2- fold increase in ALP activity on day 1, a >2-fold increase on days 3, 7, 21 and 28, and a 1.6-fold increase on day 11 when cultured in osteogenic medium compared to control medium (figure 7(b)).

4. Discussion

In this study, we optimized the generation of immortalized BMSC spheroids for printing live tissues using the Regenova 3D printer. The data illustrates that spheroids from immortalized BMSCs cultured in osteogenic media are viable and express osteogenic genes such as ALP (major enzymatic activity of osteoblasts), COL 1A1 (the main collagen expressed by osteoblasts), and OCN (the main non-collagenous protein secreted by osteoblasts and a marker of mature osteoblasts). Not only were these osteogenic genes upregulated in response to osteogenic differentiation media, but ALP activity was also increased. Furthermore, immortalized BMSC spheroids generated by centrifugation retained a higher percentage of DNA content than those that self-aggregated under gravity. BMSCs spheroids generated by centrifugation required a greater number of cells to meet the 500 µm target diameter but had ideal roundness and smoothness. Thus, the optimal spheroid fabrication technique from this study was to aggregate 40K cells under 150 – 300G centrifugation.

Previous studies have investigated the use of spheroids to produce scaffold-free tissue engineered constructs for cartilaginous tissues, such as articular cartilage, meniscus, temporomandibular joint (TMJ), and intervertebral disc[31–34], due to the similarities between condensation and differentiation that occurs during native cartilage development and the formation of the highly cellular spheroids. Cellular spheroids have also been used for scaffold-free tissue engineered cardiac, liver, skin, neural, intestine, and bone tissues[35–39]. Although 3D spheroids are not a traditional culture condition for osteogenic cells, recent studies have suggested that 3D culture is a favorable condition for promoting osteoblast maturity and enhanced osteogenic capacity[40,41]. For example, rat mesenchymal stem cell (rMSC) spheroids exhibited more osteogenic potential when compared to monolayer rMSCs. Furthermore, rMSC spheroids engrafted in rat calvarial defects demonstrated efficient bone regeneration[41]. Although these spheroids were not characterized or optimized for use in 3D printing, these results suggest that scaffold-free, spheroid-based tissue engineering may be a promising technique for bone regeneration.

Additional supplements to the osteogenic medium could enhance differentiation in future studies, but care must be taken in selecting growth factors for multipotent stem cells in 3D culture. For example, bone morphogenetic proteins (BMPs) possess osteoconductive properties that have been extensively studied in both the laboratory and clinic, but they also promote chondrogenesis. Reports in the literature demonstrate the multi-potency of BMP-2, BMP-6 and BMP-7 in directing osteogenic and chondrogenic differentiation of mesenchymal stem cells[42–47]. BMP-6 in particular has been shown to enhance osteogenesis or chondrogenesis depending on the culture conditions; BMP-6 upregulated markers of osteogenesis in adipose-derived mesenchymal stem cells in 2D monolayer and induced a chondrogenic response when the cells were cultured in 3D spheroids in the same medium[48]. These results suggest that additional supplements to the osteogenic differentiation media should be tested and optimized for 3D culture, as they may elicit a distinct response from that of 2D culture.

In this study, we optimized the fabrication of BMSC spheroids for bioprinting via the Kenzan method with the Regenova 3D printing system. We also demonstrated that the BMSCs undergo osteogenic differentiation in high-density 3D spheroid culture; this is a critical preliminary step towards using these cells to generate constructs for bone repair. However, when forming a larger construct, it may be necessary to promote spheroid fusion first, then to induce osteogenic differentiation. In the future, this bioprinting system could be used to fabricate 3D constructs for cranial reconstruction. Although the scale and complexity of bioprinting is not, at this time, able to replace complete bones, potential short-term applications for spheroid-based tissues bioprinted using the Kenzan method include implanting these tissues to fill a critical size defect. For these applications, the bioprinted tissues may require longer-term maturation and advanced conditioning to ensure they are strong enough to secure in place or they may require a supporting matrix to support the tissue. The tissues may also be used as fillers in the porous regions of metal or ceramic implants where they may augment implant integration with the host bone while the metal or ceramic implants can provide mechanical support to the biofabricated tissues.

5. Conclusion

We characterized immortalized murine BMSC spheroids using two methods of cell aggregation (gravity or centrifugation) and two types of media (control or osteogenic) to generate spheroids for 3D bioprinting on the Regenova scaffold-free printing system. This is an important first step prior to proceeding with printing of larger constructs. Overall, our findings suggest that BMSCs form viable spheroids with osteogenic gene expression increasing over time and elevated levels of alkaline phosphatase activity. BMSC spheroids produced with the centrifugation method demonstrated tighter spheroid formation with ideal roundness and smoothness. Here it was determined that the optimal spheroid fabrication technique was to aggregate 40K cells under 150 – 300G centrifugation. The next steps are to print 3D tissue

constructs using the Regenova system, characterize the large tissues prior to implantation in cranial defects in mice, and assess bone regeneration *in vivo*.

Acknowledgments

This work was supported by the Department of Orthopaedic Surgery, Indiana University School of Medicine (MAK), NIH T32AR065971 (INA), NIH S10OD023595 (LJS), and NIH T32 DK007519 (DJO). This research was also made possible by Indiana University Health and the Indiana Clinical and Translational Sciences Institute, funded in part by grant #ULI TR001108 from the National Institutes of Health, National Center for Advancing Translational Sciences, Clinical and Translational Sciences Award and The Advanced in Medicine (AIM) grant from Cook Medical (LJS). The content is solely the responsibility of the authors and does not necessarily represent the official views of the National Institutes of Health or Cook Medical. We would like to thank Dr. David Burr, Dr. Nicanor Moldovan, and the Indiana University School of Medicine 3D Bioprinting Core for their assistance and support of this project. We would also like to thank Riley Gorden, S. Ghazal Hosseini, Huseyin E. Arman, and Dr. Kevin A. Maupin for their technical assistance, and Shatoria Lunsford for her administrative support.

Figure Legends

Figure 1: The Importance of Spheroid Size

(a) Optimally-sized 500 μm spheroids are spaced on the Kenzan needle array to facilitate spheroid-spheroid contact and thus spheroid fusion. (b) and (c) Oversized spheroids interfere with one-another such that each preceding spheroid is pushed out of position during placement of adjacent spheroids. This phenomenon reduces dimensional accuracy of the construct and undermines bioprinting results. (d) Undersized spheroids do not contact one another and therefore do not fuse to one another, resulting in a failed construct. Undersized spheroids are also prone to splitting on the Kenzan needles and falling from the array, resulting in gaps in the construct.

Figure 2: Spheroid Diameter

Diameter of gravity-induced spheroids (a) in control medium at different numbers per well on day 3 (n=3). Representative silhouettes of gravity-induced spheroids with Regenova scanner for both (b) control and (c) osteogenic media. Parameters of the exponential decay equation (3) were fit to the average spheroid diameter data. Percent cell viability for both control and osteogenic spheroids is shown below diameter curve fit (n=4).

Figure 3: Histology (H&E)

Upper panel shows the gravity-induced control and osteogenic spheroids at 10X (Bar=100 μm). Lower panel shows a representation of control and osteogenic spheroids at 40X (Bar=50 μm).

Figure 4: mRNA Expression

(a) Normalized average ALP mRNA expression over 28 days. (b) Normalized average COL 1A1 mRNA expression over 28 days. (c) Normalized average OCN mRNA expression over 28 days. Eight spheroids were collected per replicate (n=3). (*) represents p values less than 0.05 when compared to control at the same time point.

Figure 5: DNA Content

DNA content over time for both gravity-and centrifugation induced spheroids. ■ Gravity control spheroids. ▲Gravity osteogenic spheroids. ● Centrifuged control spheroids. ♦ Centrifuged osteogenic spheroids. Four spheroids were collected per replicate (n=3). Data were normalized to day 0. The parameters of the exponential decay equation (4) were fit to the DNA kinetic profile.

Figure 6: Diameter on Day 3

(a) Silhouette representations of gravity- and centrifuge-induced spheroids at two different speeds (150G and 300G). □ Gravity-induced spheroids (n=3). ■ Spheroids made at 150G (n=8). ■ Spheroids made at 300G (n=8). (b) Diameter (μm) of different cell numbers. (c) Spheroid roundness for different cell numbers. (d) Spheroid smoothness for different cell numbers.

Figure 7: Alkaline Phosphatase Activity

■ Control spheroids. ■ Osteogenic spheroids. (a) ALP activity normalized to DNA over time for gravity induced spheroids. (b) ALP normalized to DNA over time for spheroids formed under centrifugation at 300G. Four spheroids were collected per replicate (n=3). (*) represents p values less than 0.05 when compared to control at the same time point.

References

1 Jiang T, Munguia-Lopez JG, Flores-Torres S, Grant J, Vijayakumar S, Leon-Rodriguez A De, *et al.* Directing the Self-Assembly of Tumour Spheroids by Bioprinting Cellular Heterogeneous Models within Alginate/Gelatin Hydrogels. *Sci Rep* 2017. https://doi.org/10.1038/s41598-017-04691-9.

2 Ozbolat IT. Scaffold-Based or Scaffold-Free Bioprinting: Competing or Complementing Approaches? *J Nanotechnol Eng Med* 2015. https://doi.org/10.1115/1.4030414.

3 Williams DF. On the mechanisms of biocompatibility. *Biomaterials* 2008. https://doi.org/10.1016/j.biomaterials.2008.04.023.

4 Norotte C, Marga FS, Niklason LE, Forgacs G. Scaffold-free vascular tissue engineering using bioprinting. *Biomaterials* 2009. https://doi.org/10.1016/j.biomaterials.2009.06.034.

5 Tesfamariam B. Bioresorbable vascular scaffolds: Biodegradation, drug delivery and vascular remodeling. *Pharmacol Res* 2016. https://doi.org/10.1016/j.phrs.2016.03.020.

6 Matsusaki M, Kadowaki K, Tateishi K, Higuchi C, Ando W, Hart DA, *et al.* Scaffold-Free Tissue-Engineered Construct–Hydroxyapatite Composites Generated by an Alternate Soaking Process: Potential for Repair of Bone Defects. *Tissue Eng Part A* 2009. https://doi.org/10.1089/ten.tea.2007.0424.

7 Pourchet LJ, Thepot A, Albouy M, Courtial EJ, Boher A, Blum LJ, *et al.* Human Skin 3D Bioprinting Using Scaffold-Free Approach. *Adv Healthc Mater* 2017. https://doi.org/10.1002/adhm.201601101.

8 Shimomura K, Ando W, Fujie H, Hart DA, Yoshikawa H, Nakamura N. Scaffold-free tissue engineering for injured joint surface restoration. *J Exp Orthop* 2018. https://doi.org/10.1186/s40634-017-0118-0.

9 Shimoto T, Nakayama K, Matsuda S, Iwamoto Y. Building of HD MACs using cell processing robot for cartilage regeneration. *J Robot Mechatronics* 2012. https://doi.org/10.20965/jrm.2012.p0347.

10 Itoh M, Nakayama K, Noguchi R, Kamohara K, Furukawa K, Uchihashi K, *et al.* Scaffold-free tubular tissues created by a bio-3D printer undergo remodeling and endothelialization when implanted in rat aortae. *PLoS One* 2015. https://doi.org/10.1371/journal.pone.0136681.

11 Machnio R, Matsumoto K, Taura Y, Yamasaki N, Tagagi K, Tsuchiya T, *et al.* Scaffold-Free Trachea Tissue Engineering Using Bioprinting.

12 Moldovan L, Barnard A, Gil CH, Lin Y, Grant MB, Yoder MC, *et al.* iPSC-Derived Vascular Cell Spheroids as Building Blocks for Scaffold-Free Biofabrication. *Biotechnol J* 2017;**12**:1–25. https://doi.org/10.1002/biot.201700444.

13 Taniguchi D, Matsumoto K, Tsuchiya T, MacHino R, Takeoka Y, Elgalad A, *et al.* Scaffold-free trachea regeneration by tissue engineering with bio-3D printing. *Interact Cardiovasc Thorac Surg* 2018. https://doi.org/10.1093/icvts/ivx444.

14 Mironov V, Visconti RP, Kasyanov V, Forgacs G, Drake CJ, Markwald RR. Organ

printing: Tissue spheroids as building blocks. *Biomaterials* 2009. https://doi.org/10.1016/j.biomaterials.2008.12.084.
15 Yu Y, Ozbolat IT. Tissue Strands as 'Bioink' for Scale-up Organ Printing.
16 Robinson EE. alpha5beta1 integrin mediates strong tissue cohesion. *J Cell Sci* 2003. https://doi.org/10.1242/jcs.00231.
17 Gentile C, Fleming PA, Mironov V, Argraves KM, Argraves WS, Drake CJ. VEGF-mediated fusion in the generation of uniluminal vascular spheroids. *Dev Dyn* 2008. https://doi.org/10.1002/dvdy.21720.
18 Bao B, Jiang J, Yanase T, Nishi Y, Morgan JR. Connexon-mediated cell adhesion drives microtissue self-assembly. *FASEB J* 2011. https://doi.org/10.1096/fj.10-155291.
19 Teo WE, He W, Ramakrishna S. No Title. *Biotechnol J* 2006;**1**:918.
20 Ahmad T, Lee J, Shin YM, Shin HHJ, Madhurakat Perikamana SK, Park SH, *et al.* Hybrid-spheroids incorporating ECM like engineered fragmented fibers potentiate stem cell function by improved cell/cell and cell/ECM interactions. *Acta Biomater* 2017. https://doi.org/10.1016/j.actbio.2017.10.022.
21 Griffin FE, Schiavi J, McDevitt TC, McGarry JP, McNamara LM. The role of adhesion junctions in the biomechanical behaviour and osteogenic differentiation of 3D mesenchymal stem cell spheroids. *J Biomech* 2017. https://doi.org/10.1016/j.jbiomech.2017.05.014.
22 Ong CS, Yesantharao P, Huang CY, Mattson G, Boktor J, Fukunishi T, *et al.* 3D bioprinting using stem cells. *Pediatr Res* 2017. https://doi.org/10.1038/pr.2017.252.
23 Xia JJ, Gateno J, Teichgraeber JF. New Clinical Protocol to Evaluate Craniomaxillofacial Deformity and Plan Surgical Correction. *J Oral Maxillofac Surg* 2009. https://doi.org/10.1016/j.joms.2009.04.057.
24 Campana V, Milano G, Pagano E, Barba M, Cicione C, Salonna G, *et al.* Bone substitutes in orthopaedic surgery: from basic science to clinical practice. *J Mater Sci Mater Med* 2014. https://doi.org/10.1007/s10856-014-5240-2.
25 Shang Q, Wang Z, Liu W, Shi Y, Cui L, Cao Y. Tissue-engineered bone repair of sheep cranial defects with autologous bone marrow stromal cells. *J Craniofac Surg* 2001. https://doi.org/10.1097/00001665-200111000-00017.
26 Grayson WL, Frohlich M, Yeager K, Bhumiratana S, Chan ME, Cannizzaro C, *et al.* Engineering anatomically shaped human bone grafts. *Proc Natl Acad Sci* 2010. https://doi.org/10.1073/pnas.0905439106.
27 Sundseth J, Berg-Johnsen J. Prefabricated patient-matched cranial implants for reconstruction of large skull defects. *J Cent Nerv Syst Dis* 2013. https://doi.org/10.4137/JCNSD.S11106.
28 Msallem B, Beiglboeck F, Honigmann P, Jaquiéry C, Thieringer F. Craniofacial Reconstruction by a Cost-Efficient Template-Based Process Using 3D Printing.
29 Alvarez MB, Childress P, Philip BK, Gerard-O'Riley R, Hanlon M, Herbert BS, *et al.* Immortalization and characterization of osteoblast cell lines generated from wild-type and Nmp4-null mouse bone marrow stromal cells using murine telomerase reverse transcriptase (mTERT). *J Cell Physiol* 2012. https://doi.org/10.1002/jcp.22915.
30 Patil YB, Swaminathan SK, Sadhukha T, Ma L, Panyam J. The use of nanoparticle-mediated targeted gene silencing and drug delivery to overcome tumor drug resistance. *Biomaterials* 2010. https://doi.org/10.1016/j.biomaterials.2009.09.048.
31 Babur BK, Ghanavi P, Levett P, Lott WB, Klein T, Cooper-White JJ, *et al.* The Interplay between Chondrocyte Redifferentiation Pellet Size and Oxygen Concentration. *PLoS One* 2013. https://doi.org/10.1371/journal.pone.0058865.
32 Ishihara K, Nakayama K, Akieda S, Matsuda S, Iwamoto Y. Simultaneous regeneration of full-thickness cartilage and subchondral bone defects in vivo using a three-dimensional scaffold-free autologous construct derived from high-density bone marrow-derived

mesenchymal stem cells. *J Orthop Surg Res* 2014. https://doi.org/10.1186/s13018-014-0098-z.

33 DuRaine GD, Brown WE, Hu JC, Athanasiou KA. Emergence of Scaffold-Free Approaches for Tissue Engineering Musculoskeletal Cartilages. *Ann Biomed Eng* 2015. https://doi.org/10.1007/s10439-014-1161-y.

34 Toratani T, Nakase J, Numata H, Oshima T, Takata Y, Nakayama K, *et al.* Scaffold-Free Tissue-Engineered Allogenic Adipose-Derived Stem Cells Promote Meniscus Healing. *Arthrosc - J Arthrosc Relat Surg* 2017. https://doi.org/10.1016/j.arthro.2016.07.015.

35 L'heureux N, Pâquet S, Labbé R, Germain L, Auger FA. A completely biological tissue-engineered human blood vessel. *FASEB J* 1998. https://doi.org/10.1096/fasebj.12.1.47.

36 Kale S, Biermann S, Edwards C, Tarnowski C, Morris M, Long MW. Three-dimensional cellular development is essential for ex vivo formation of human bone. *Nat Biotechnol* 2000. https://doi.org/10.1038/79439.

37 McCracken KW, Howell JC, Wells JM, Spence JR. Generating human intestinal tissue from pluripotent stem cells in vitro. *Nat Protoc* 2011. https://doi.org/10.1038/nprot.2011.410.

38 Dingle Y-TL, Boutin ME, Chirila AM, Livi LL, Labriola NR, Jakubek LM, *et al.* Three-Dimensional Neural Spheroid Culture: An *In Vitro* Model for Cortical Studies. *Tissue Eng Part C Methods* 2015. https://doi.org/10.1089/ten.tec.2015.0135.

39 Takagi R, Ishimaru J, Sugawara A, Toyoshima KE, Ishida K, Ogawa M, *et al.* Bioengineering a 3D integumentary organ system from iPS cells using an in vivo transplantation model. *Sci Adv* 2016. https://doi.org/10.1126/sciadv.1500887.

40 Jähn K, Richards RG, Archer CW, Stoddart MJ. Pellet culture model for human primary osteoblasts. *Eur Cell Mater* 2010. https://doi.org/vol020a13 [pii].

41 Yamaguchi Y, Ohno J, Sato A, Kido H, Fukushima T. Mesenchymal stem cell spheroids exhibit enhanced in-vitro and in-vivo osteoregenerative potential. *BMC Biotechnol* 2014. https://doi.org/10.1186/s12896-014-0105-9.

42 Hanada K, Dennis JE, Caplan a I. Stimulatory effects of basic fibroblast growth factor and bone morphogenetic protein-2 on osteogenic differentiation of rat bone marrow-derived mesenchymal stem cells. *J Bone Miner Res* 1997. https://doi.org/10.1359/jbmr.1997.12.10.1606.

43 Sekiya I, Colter DC, Prockop DJ. BMP-6 enhances chondrogenesis in a subpopulation of human marrow stromal cells. *Biochem Biophys Res Commun* 2001. https://doi.org/10.1006/bbrc.2001.4898.

44 Schmitt B, Ringe J, Häupl T, Notter M, Manz R, Burmester GR, *et al.* BMP2 initiates chondrogenic lineage development of adult human mesenchymal stem cells in high-density culture. *Differentiation* 2003. https://doi.org/10.1111/j.1432-0436.2003.07109003.x.

45 Toh WS, Liu H, Heng BC, Rufaihah AJ, Ye CP, Cao T. Combined effects of TGFbeta1 and BMP2 in serum-free chondrogenic differentiation of mesenchymal stem cells induced hyaline-like cartilage formation. *Growth Factors* 2005. https://doi.org/10.1080/08977190500252763.

46 Friedman MS, Long MW, Hankenson KD. Osteogenic differentiation of human mesenchymal stem cells is regulated by bone morphogenetic protein-6. *J Cell Biochem* 2006. https://doi.org/10.1002/jcb.20719.

47 Shen B, Wei A, Whittaker S, Williams LA, Tao H, Ma DDF, *et al.* The role of BMP-7 in chondrogenic and osteogenic differentiation of human bone marrow multipotent mesenchymal stromal cells in vitro. *J Cell Biochem* 2010. https://doi.org/10.1002/jcb.22412.

48 Kemmis CM, Vahdati A, Weiss HE, Wagner DR. Bone morphogenetic protein 6 drives both osteogenesis and chondrogenesis in murine adipose-derived mesenchymal cells

depending on culture conditions. *Biochem Biophys Res Commun* 2010. https://doi.org/10.1016/j.bbrc.2010.08.135.

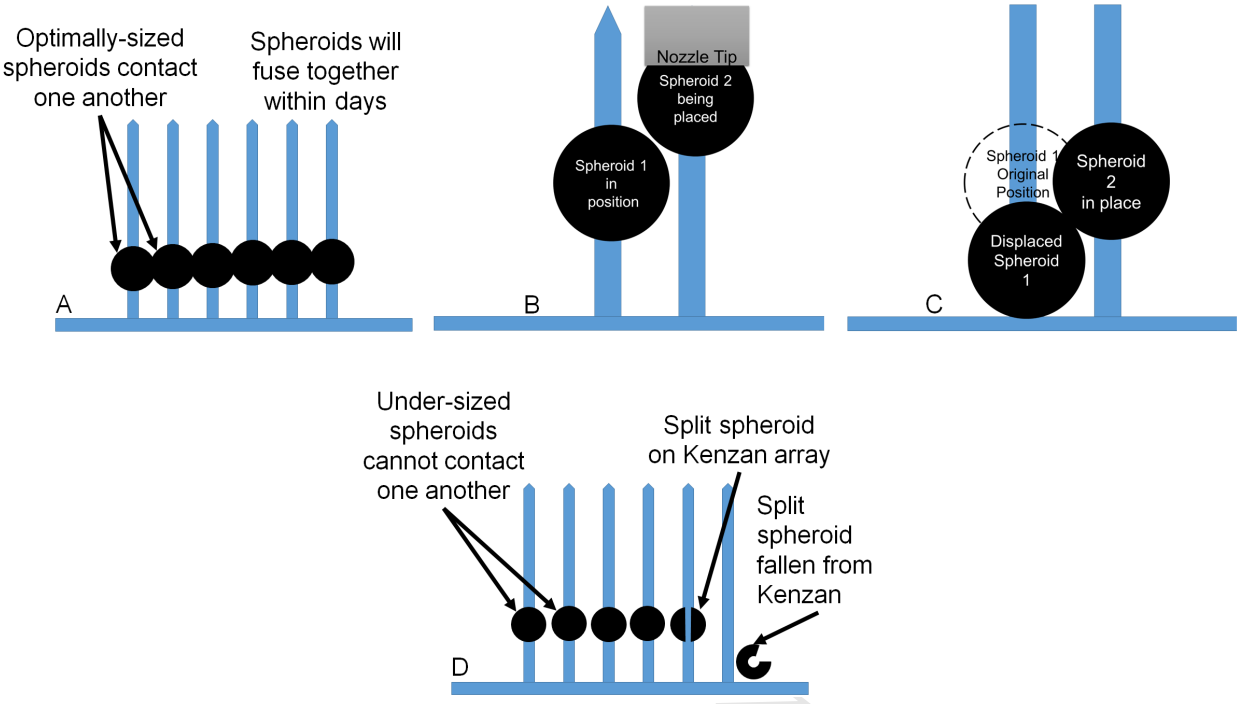

A

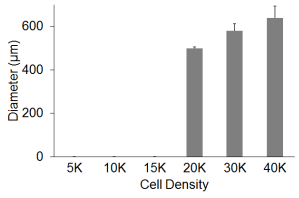

B

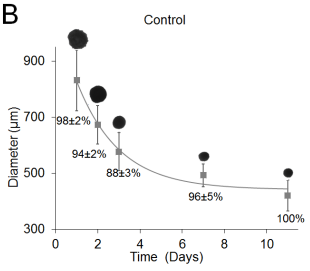

C

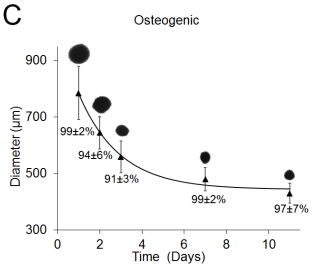

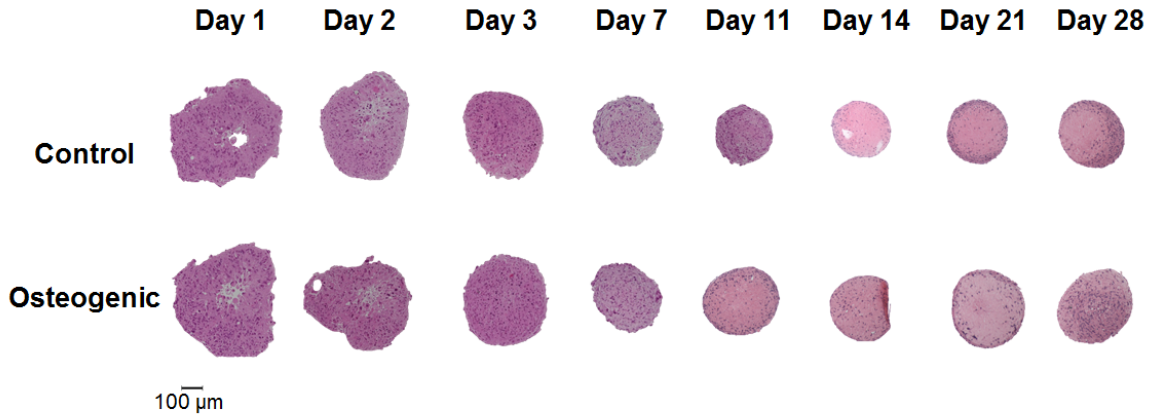
Day 1
Day 2
Day 3
Day 7
Day 11
Day 14
Day 21
Day 28
Control
Osteogenic
100 µm

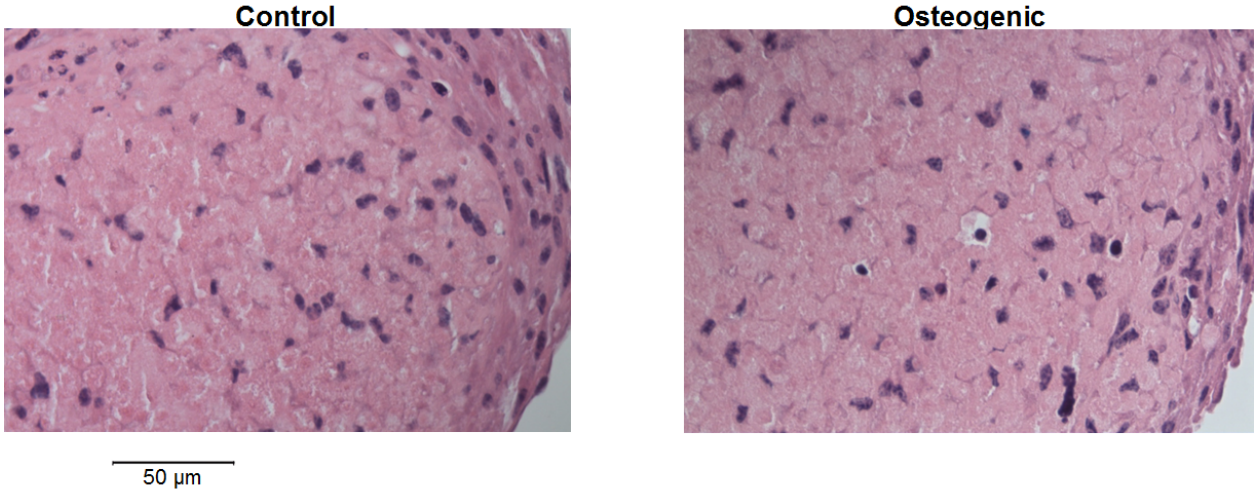
Control
Osteogenic
50 µm

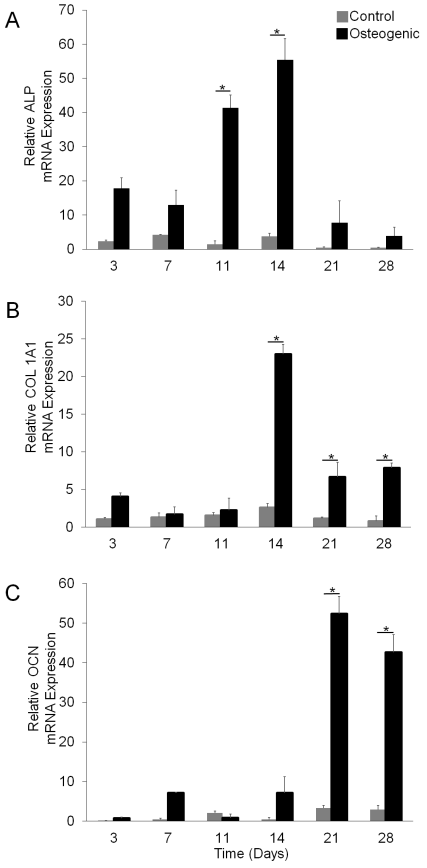

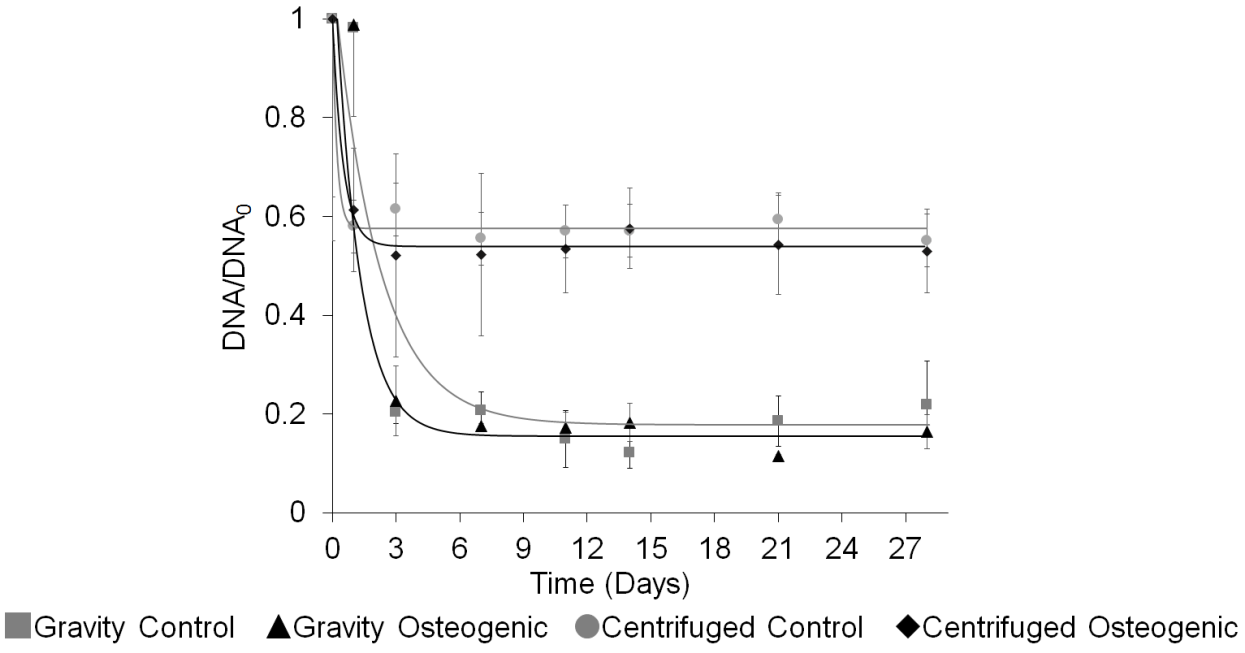

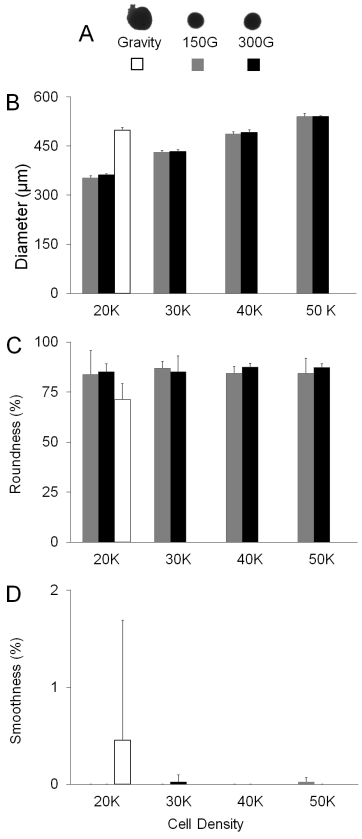

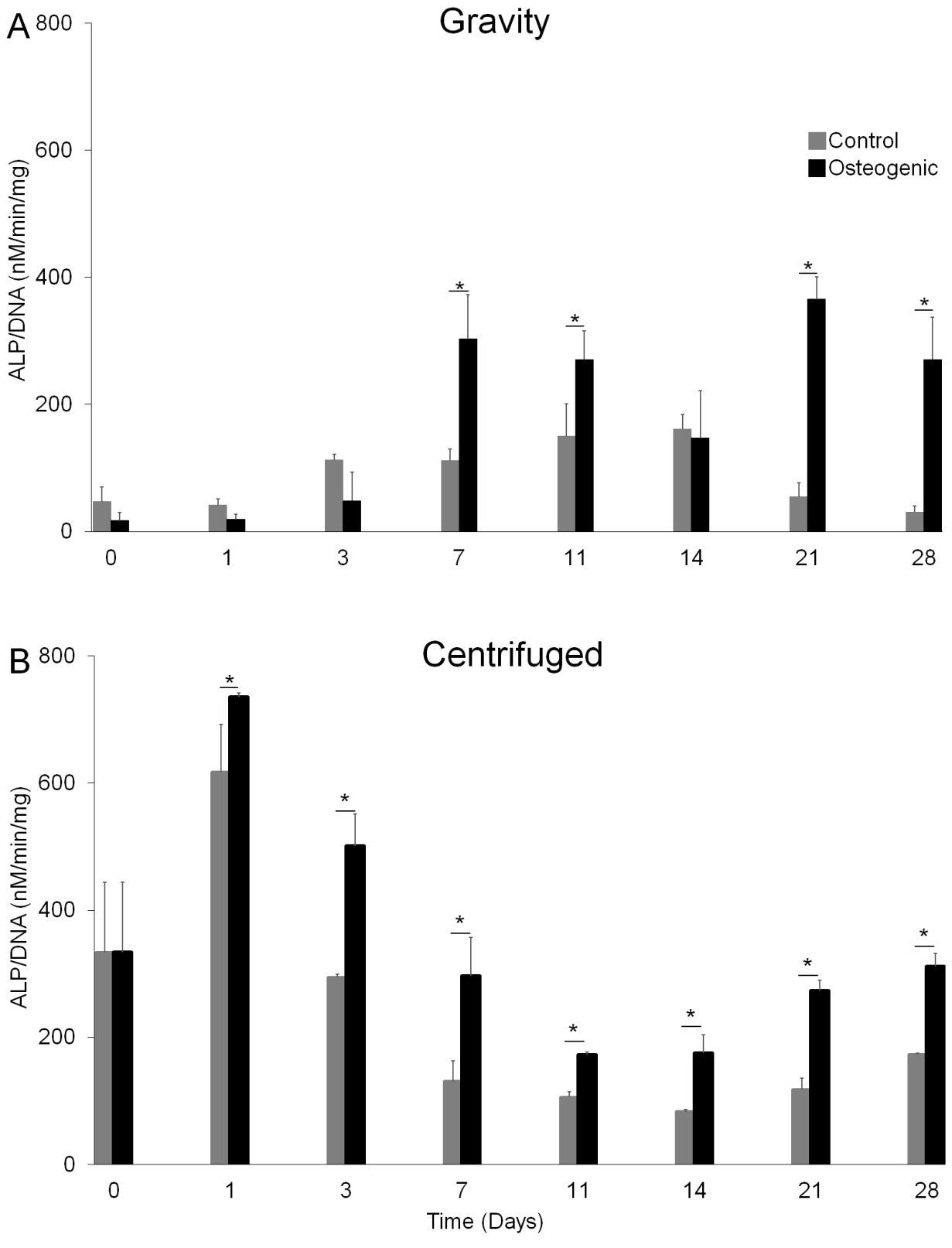
A
Gravity
ALP/DNA (nM/min/mg)
800
600
400
200
0
Control
Osteogenic
0
1
3
7
11
14
21
28
B
Centrifuged
ALP/DNA (nM/min/mg)
800
600
400
200
0
0
1
3
7
11
14
21
28
Time (Days)